DOI:
10.1109/TIFS.2016.2516917

Document Version
Publisher's PDF, also known as Version of record

Physical Layer Security in Three-Tier Wireless Sensor Networks: A Stochastic Geometry Approach

Yansha Deng, *Student Member, IEEE*, Lifeng Wang, *Member, IEEE*, Maged Elkashlan, *Member, IEEE*, Arumugam Nallanathan, *Senior Member, IEEE*, and Ranjan K. Mallik, *Fellow, IEEE*

***Abstract*— This paper develops a tractable framework for exploiting the potential benefits of physical layer security in three-tier wireless sensor networks (WSNs) using stochastic geometry. In such networks, the sensing data from the remote sensors are collected by sinks with the help of access points, and the external eavesdroppers intercept the data transmissions. We focus on the secure transmission in two scenarios: 1) the active sensors transmit their sensing data to the access points and 2) the active access points forward the data to the sinks. We derive new compact expressions for the average secrecy rate in these two scenarios. We also derive a new compact expression for the overall average secrecy rate. Numerical results corroborate our analysis and show that multiple antennas at the access points can enhance the security of three-tier WSNs. Our results show that increasing the number of access points decreases the average secrecy rate between the access point and its associated sink. However, we find that increasing the number of access points first increases the overall average secrecy rate, with a critical value beyond which the overall average secrecy rate then decreases. When increasing the number of active sensors, both the average secrecy rate between the sensor and its associated access point, and the overall average secrecy rate decrease. In contrast, increasing the number of sinks improves both the average secrecy rate between the access point and its associated sink, and the overall average secrecy rate.**

***Index Terms*— Beamforming, decode-and-forward (DF), physical layer security, stochastic geometry, wireless sensor networks (WSNs).**

I. Introduction

DUE TO its wide applications such as environmental sensing, health monitoring, and military communications [2], wireless sensor networks (WSNs) have attracted considerable attention from the industry and academia. The security of WSNs is a big concern, since the broadcast nature of wireless channels is susceptible to eavesdropping and the sensing data needs to be protected. In practice, the small-size, low-cost and low-power sensors are randomly deployed to sense the data, which is sent back to the sinks by multihop transmissions. Multihop architectures pose great challenges to conventional cryptographic methods involving key distribution and management, and result in high complexity in data encryption and decryption. Physical layer security has emerged as an appealing low-complexity approach to secure the information transmission. The core idea behind it is to exploit the characteristics of wireless channels such as fading or noise to transmit a message from a source to an intended destination while keeping the message confidential from eavesdroppers. Motivated by this, the potential applications of physical layer security have been investigated in various wireless networks such as cellular networks, cognitive radio, ad-hoc, etc.

Manuscript received April 27, 2015; revised November 21, 2015; accepted January 1, 2016. Date of publication January 19, 2016; date of current version March 16, 2016. This work was supported by the U.K. Engineering and Physical Sciences Research Council under Grant EP/M016145/1. This paper was presented in part at the IEEE Global Communications Conference, San Diego, CA, Dec. 2015 [1]. The associate editor coordinating the review of this manuscript and approving it for publication was Prof. T. Charles Clancy.

Y. Deng and A. Nallanathan are with the Department of Informatics, King's College London, London WC2R 2LS, U.K. (e-mail: yansha.deng@kcl.ac.uk; arumugam.nallanathan@kcl.ac.uk).

L. Wang is with the Department of Electronic and Electrical Engineering, University College London, London WC1E 6BT, U.K. (e-mail: lifeng.wang@ucl.ac.uk).

M. Elkashlan is with the School of Electronic Engineering and Computer Science, Queen Mary University of London, London E1 4NS, U.K. (e-mail: maged.elkashlan@qmul.ac.uk).

R. K. Mallik is with the Department of Electrical Engineering, IIT Delhi, New Delhi 110016, India (e-mail: rkmallik@ee.iitd.ernet.in).

Color versions of one or more of the figures in this paper are available online at http://ieeexplore.ieee.org.

Digital Object Identifier 10.1109/TIFS.2016.2516917

A. Physical Layer Security: Current State-of-the-Art

In the 1970s, Wyner first introduced physical layer security [3]. Triggered by the rapid evolution of wireless network architectures, the idea of enabling security at physical layer has drawn the attention of the wireless community [4]. In cellular networks, physical layer security is important for adding an extra level of protection [5], [6]. In [5], secure downlink transmission in cellular networks was investigated, and the secrecy using linear precoding based on regularized channel inversion was examined. In multi-cell environments, the cell association and location information of mobile users play an important role in secrecy performance [6]. Although it can alleviate the scarcity of radio frequency spectrum, security of cognitive radio networks is critical as it is easily exposed to external threats [7], [8]. In [7], the optimal secrecy beamforming in a multiple-input single-output (MISO) cognitive radio wiretap channel was proposed. The beamforming and artificial noise was proposed to enhance the secure transmission of large scale spectrum sharing networks [8]. In cooperative networks, relays are deployed to boost the coverage and reliability, however, the relay can be trusted [9], [10] or untrusted [11] where the untrusted relay is thought of as an eavesdropper. In [9], the design of trusted relay weights and allocation of transmit power under different relay protocols such as amplify-and-forward (AF), decode-and-forward (DF), and cooperative jamming (CJ) was considered. In [10], trusted relay selection schemes based on the AF and DF protocols were proposed to improve physical layer security. In untrusted relay networks, CJ was introduced to confuse the untrusted relay [11].

In decentralized networks such as ad-hoc, the public-key cryptography is expensive and difficult [12]–[14]. In [12], the secure connectivity in wireless random networks was studied, and the eigen-beamforming was implemented to maximize the signal strength to the intended receiver. In [13], the secrecy transmission capacity in wireless ad-hoc networks was analyzed, and the secrecy guard zone was introduced to improve the secrecy transmission capacity. In [14], the transmit beamforming with artificial noise strategies were used to enhance the secrecy in large-scale ad-hoc networks. In [15], the secure communication in twotier heterogeneous networks (HetNets) was enhanced through massive multiple-input multiple-output (MIMO).

Physical layer security schemes have been recently proposed for WSNs to combat eavesdropping [16]–[19]. In [16], the downlink secure transmission from the mobile agent to the authorized user was considered and perfect secrecy can be achieved by intentionally creating channel variation. In [17], a detection problem under physical layer secrecy constraints in an energy-constrained WSNs was addressed, and the optimal operative solutions were analyzed. In [18], sensor transmissions were observed by the authorized fusion center (FC) and unauthorized (third party) FC. It was shown that physical layer security for distributed detection is scalable due to its low computational complexity. More recently in [19], compressed sensing (CS) was introduced to provide secrecy against eavesdropping in addition to the other CS benefits.

B. Approach and Contributions

In this paper, we examine the potential benefits of physical layer security in a three-tier WSN using stochastic geometry modeling. In three-tier WSNs, the sensors are located far from the sinks, and the access points are deployed to help the sensors forward their data to the sinks. Confidential information transmissions are intercepted by the eavesdroppers. Considering the fact that sensors are densely deployed and their locations are randomly distributed [2], we introduce stochastic geometry to model the locations of the nodes in WSNs. Such a modeling approach has been applied in heterogeneous networks [20] and cognitive radio networks [21]. Our main contributions are summarized as follows.

- We develop a new analytical framework to examine the implementation of physical layer security in three-tier WSNs. The locations and spatial densities of sensors, access points, sinks, and eavesdroppers are modeled using stochastic geometry. Each access point is equipped with multiple antennas and uses the low-complexity maximal-ratio combining (MRC) to receive the data signals from the sensors and maximal-ratio transmission (MRT) beamformer to transmit the signals. We investigate the secure transmissions between the active sensors and access points, and beween the active access points and sinks.
- We present new statistical properties, based on which we derive new compact expressions for the average secrecy rate between the typical sensor and its associated access point, and between the typical access point and its associated sink. We also derive the minimum number of sinks required for a target average secrecy rate. Particularly, we derive a new compact expression for overall average secrecy rate in three-tier WSNs.
- We show that using MRC/MRT at access points can enhance the secure transmission. Based on the proposed analysis and simulations, several important observations are reached: 1) the average secrecy rate decreases as the number of sensors grows large, due to more interference from sensors, 2) the average secrecy rate increases with increasing the number of sinks, because of the shorter distances between the access points and their associated sinks, and 3) the overall average secrecy rate increases with increasing the number of access points. However, beyond a critical value, the overall average secrecy rate decreases with increasing the number of access points.

The notation of this paper is given in Table I.

TABLE I
NOTATION

$\Phi_{s,a}$	Poison point process (PPP) of sensor locations
λ_s	Intensity of Φ_s
$\Phi_{ap,a}$	PPP of access points locations
λ_{ap}	Intensity of Φ_{ap}
Φ_{sk}	PPP of sinks locations
λ_{sk}	Intensity of Φ_{sk}
ρ_s	The probability that sensor is triggered to transmit the data
ρ_{ap}	The activity probability of access point that forwards the data to the sinks
$\Phi_{s,e}$	PPP of eavesdropper locations, where the eavesdroppers intercept the sensors' data
$\Phi_{ap,e}$	PPP of eavesdropper locations, where the eavesdroppers intercept the access points' data
λ_e^s	Intensity of $\Phi_{s,e}$
λ_e^{ap}	Intensity of $\Phi_{ap,e}$
$\dagger$	Conjugate transpose

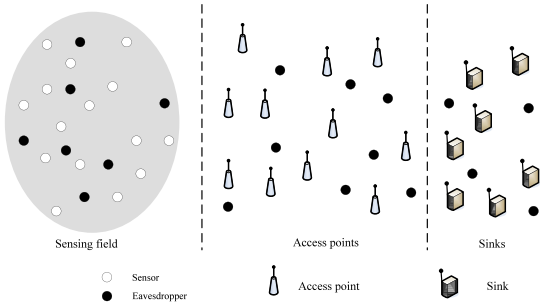

Fig. 1. Illustration of three-tier wireless sensor networks, where the sensors transmit the data to the sinks via the access points, in the presence of eavesdropping.

II. SYSTEM DESCRIPTION

As shown in Fig. 1, a three-tier WSN is considered, where the geographically remote sensors transmit the sensed data to the sinks with the help of half-duplex decode-and-forward (DF) access points with no direct links between sensors and sinks. The eavesdroppers overhears the data transmission without modifying it. In the sensing field, sensors are randomly located according to a homogeneous Poisson point process (HPPP) Φ_s with intensity λ_s. In order to consider unplanned deployment of the access points and sinks,

the random locations of the access points and sinks are approximated as independent HPPPs Φ_{ap} and Φ_{sk} with intensities λ_{ap} and λ_{sk}, respectively, which is suitable in large scale networks [22]. Since the sensors may transmit data intermittently, the activity probability of a sensor that is triggered to transmit the data is denoted as ρ_s $(0 < \rho_s < 1)$, and the activity probability of an access point that forwards the data to the sink is denoted as ρ_{ap} $(0 < \rho_{ap} < 1)$.[1] We assume that the probability of being an active sensor/access point is independent of the access point/sink's location. Therefore, the active sensors and active access points constitute independent HPPPs $\Phi_{s,a}$ and $\Phi_{ap,a}$ with intensities $\lambda_s\rho_s$ and $\lambda_{ap}\rho_{ap}$, respectively [22]. Non-colluding eavesdroppers are considered and eavesdroppers' locations are modeled as two independent HPPPs $\Phi_{s,e}$ and $\Phi_{ap,e}$ with intensities λ_e^s and λ_e^{ap}, respectively. The eavesdroppers in $\Phi_{s,e}$ intercept the data transmitted by the sensors and the eavesdroppers in $\Phi_{ap,e}$ intercept the data transmitted by the access points. Note that the eavesdroppers in $\Phi_{s,e}$ and in $\Phi_{ap,e}$ are far from each other.

In this three-tier network, the sensor is associated with its nearest access point to receive the sensor's data and the access point is associated with its nearest sink to receive the access point's data.[2] Each access point is equipped with M antennas, and the sensors and sinks are single-antenna nodes. To enhance the information transmission, the access points use MRC to receive the sensors' data signals and MRT beamformer to transmit the signals. The wireless channels are modeled as independent quasi-static Rayleigh fading.

An arbitrary typical sensor o transmits data to its nearest access point (called typical access point). The typical access point not only receives the useful data from the typical sensor, but is also subject to the interference from other active sensors and active access points. Thus, the receive signal-to-interference-plus-noise ratio (SINR) after MRC at its corresponding typical access point is given by

$$\gamma_{ap} = \frac{\left\|\mathbf{h}_{s_0,ap_0}\right\|^2 \left|X_{s_0,ap_0}\right|^{-\alpha}}{\underbrace{I_{s,ap} + I_{ap,ap}}_{In_{ap}} + \delta^2/P_s}, \tag{1}$$

where $I_{s,ap} = \sum_{i\in\Phi_{s,a}\setminus\{s_0\}} \left|\frac{\mathbf{h}_{s_0,ap_0}^{\dagger}}{\|\mathbf{h}_{s_0,ap_0}\|}\mathbf{h}_{i,ap_0}\right|^2 |X_{i,ap_0}|^{-\alpha}$, $I_{ap,ap} = \mu\sum_{j\in\Phi_{ap,a}\setminus\{ap_0\}} \left|\frac{\mathbf{h}_{s_0,ap_0}^{\dagger}}{\|\mathbf{h}_{s_0,ap_0}\|}\mathbf{H}_{j,ap_0}\frac{\mathbf{h}_{j,sk_j}^{\dagger}}{\|\mathbf{h}_{j,sk_j}\|}\right|^2 |X_{j,ap_0}|^{-\alpha}$, and $\mu = P_{ap}/P_s$. Note that the interfering access points deliver their own data to their corresponding sinks using MRT beamformer vector $\frac{\mathbf{h}_{j,sk_j}^{\dagger}}{\|\mathbf{h}_{j,sk_j}\|}$, which are also received and combined at the typical access point with MRC vector $\frac{\mathbf{h}_{s_0,ap_0}^{\dagger}}{\|\mathbf{h}_{s_0,ap_0}\|}$. Here, $\mathbf{h}_{s_0,ap_0}$ and $|X_{s_0,ap_0}|$ are the channel fading vector and distance between the typical sensor and its typical access point, respectively, α is the path loss exponent, $\mathbf{h}_{i,ap_0} \in \mathcal{C}^{M\times 1}$ and $|X_{i,ap_0}|$ are the channel fading vector and distance between the sensor i and the typical access point, respectively, $\mathbf{H}_{j,ap_0}$ and $|X_{j,ap_0}|$ are the channel fading matrix and distance between the interfering access point j and the typical access point, respectively, $\mathbf{h}_{j,sk_j} \in \mathcal{C}^{1\times M}$ is the channel fading vector between the interfering access point j and its corresponding sink, P_s is the sensor's transmit power, P_{ap} is the access point's transmit power, and δ^2 is the noise power.

We consider the non-colluding eavesdropping scenario, in which the most detrimental eavesdropper that has the highest receive SINR dominates the secrecy rate [9]. An arbitrary eavesdropper e_k that intercepts the sensor and the access point transmission overhears the useful signal from the typical sensor to the typical access point, and simultaneously receives the interfering data from the other active sensors and active access points. This eavesdropper suffers from the interfering signals emitted by the other interfering access points using the MRT beamformer $\frac{\mathbf{h}_{j,sk_k}^{\dagger}}{\|\mathbf{h}_{j,sk_k}\|}$. Thus, the received SINR at the most detrimental eavesdropper in $\Phi_{s,e}$ for the sensor and the access point transmission is given by

$$\gamma_{s,e} = \max_{e_k\in\Phi_{s,e}} \left\{ \frac{\left|h_{s_0,e_k}\right|^2 \left|X_{s_0,e_k}\right|^{-\alpha}}{\underbrace{I_{s,e} + I_{ap,e}}_{In_{s,e}} + \delta^2/P_s} \right\}, \tag{2}$$

where $I_{s,e} = \sum_{i\in\Phi_{s,a}\setminus\{s_0\}} |h_{i,e_k}|^2 |X_{i,e_k}|^{-\alpha}$ and $I_{ap,e} = \sum_{j\in\Phi_{ap,a}\setminus\{ap_0\}} \mu \left|\mathbf{h}_{j,e_k}\frac{\mathbf{h}_{j,sk_j}^{\dagger}}{\|\mathbf{h}_{j,sk_j}\|}\right|^2 |X_{j,e_k}|^{-\alpha}$, h_{s_0,e_k} and $|X_{s_0,e_k}|$ are the channel fading coefficient and distance between the typical sensor and the eavesdropper, respectively, h_{i,e_k} and $|X_{i,e_k}|$ are the channel fading coefficient and distance between sensor i and the eavesdropper, respectively, and $\mathbf{h}_{j,e_k}$ and $|X_{j,e_k}|$ are the channel fading vector and distance between the access point j and the eavesdropper, respectively.

After receiving the typical sensor's data, the typical access point ap_0 will forward the sensed data to the nearest sink (called typical sink) sk_0 for data collection. Due to the current transmission from other active access points, the typical sink suffers from their interferences. As such, the received SINR at the typical sink sk_0 is given by

$$\gamma_{sk} = \frac{\left\|\mathbf{g}_{ap_0,sk_0}\right\|^2 \left|X_{ap_0,sk_0}\right|^{-\beta}}{In_{ap,sk} + \delta^2/P_{ap}}, \tag{3}$$

where $In_{ap,sk} = \sum_{j\in\Phi_{ap,a}\setminus\{ap_0\}} \left|\mathbf{g}_{j,sk_0}\frac{\mathbf{h}_{j,sk_j}^{\dagger}}{\|\mathbf{h}_{j,sk_j}\|}\right|^2 |X_{j,sk_0}|^{-\beta}$, $\mathbf{g}_{ap_0,sk_0} \in \mathcal{C}^{1\times M}$ and $|X_{ap_0,sk_0}|$ are the channel fading vector and distance between the typical access point and its typical sink, respectively, β is the path loss exponent, $\mathbf{g}_{j,sk_0} \in \mathcal{C}^{1\times M}$ and $|X_{j,sk_0}|$ are the channel fading vector and distance between the access point j and the typical sink, and $\mathbf{h}_{j,sk_j} \in \mathcal{C}^{1\times M}$ is the channel fading vector between the access point j and its associated sink.

[1] In practical scenarios, the access points operate in three modes: receiving the sensed data from active sensors, forwarding the sensed data to the sinks, and idle. The activity probability of sensor only determines the number of access points which receive the data from the active sensors, and is independent of the number of access points which forward the data to the sink. The number of active access points that are triggered to forward the sensed data to sinks depends on the availability of sinks. As such, ρ_s and ρ_{ap} are independent values.

[2] In reality, there may be more than one active sensor/access point to choose the same access point/sink; this can be effectively dealt with using multiple access techniques.

An arbitrary eavesdropper e_k that intercepts the typical access point and the typical sink transmission overhears the signal transmitted by the typical access point with the MRT beamformer $\frac{\mathbf{g}_{ap_0,sk_0}{}^{\dagger}}{\|\mathbf{g}_{ap_0,Sk_0}\|}$, and suffers from the interfering signals emitted by other interfering access points with the MRT beamformer $\frac{\mathbf{h}_{j,sk_k}{}^{\dagger}}{\|\mathbf{h}_{j,sk_k}\|}$. Thus, the received SINR at the most detrimental eavesdropper for the access point and the sink transmission is given by

$$\gamma_{ap,e} = \max_{e_k \in \Phi_{ap,e}} \left\{ \frac{\left| \mathbf{g}_{ap_0,e_k} \frac{\mathbf{g}_{ap_0,sk_0}{}^{\dagger}}{\|\mathbf{g}_{ap_0,Sk_0}\|} \right|^2 \left| X_{ap_0,e_k} \right|^{-\beta}}{In_{ap,e} + \sigma^2/P_{ap}} \right\}, \quad (4)$$

where $In_{ap,e} = \sum_{j \in \Phi_{ap,a} \setminus \{ap_0\}} \left| \mathbf{g}_{j,e_k} \frac{\mathbf{h}_{j,sk_k}{}^{\dagger}}{\|\mathbf{h}_{j,sk_k}\|} \right|^2 |X_{j,e_k}|^{-\beta}$, g_{ap_0,e_k} and $|X_{ap_0,e_k}|$ are the channel fading coefficient and distance between the typical access point and the eavesdropper, respectively, and $\mathbf{g}_{j,e_k}$ and $|X_{j,e_k}|$ are the channel fading vector and distance between the access point j and the eavesdropper, respectively.

III. Secrecy Performance Evaluations

In this section, we characterize the secrecy performance in terms of average secrecy rate. Before exhibiting the overall secrecy performance behaviors, we evaluate the secrecy of two different links, namely the link between the sensor and access point, and the link between the access point and sink. We derive new analytical expressions for the average secrecy rate, and analyze the impact of the two links on the overall average secrecy rate.

A. Average Secrecy Rate Between Sensor and Access Point

We evaluate the average secrecy rate based on the worst-case, where the eavesdropper with the best SINR is used to calculate the average secrecy rate [9]. Hence, for a typical link between a typical sensor and its associated access point, the instantaneous secrecy rate is defined as [23]

$$C_s^{ap} = [C_{ap} - C_{s,e}]^+, \quad (5)$$

where $[x]^+ = \max\{x, 0\}$, $C_{ap} = \log_2\left(1 + \gamma_{ap}\right)$ is the capacity of the channel between the typical sensor and access point, and $C_{s,e} = \log_2\left(1 + \gamma_{s,e}\right)$ is the capacity of the eavesdropping channel between the typical sensor and the most detrimental eavesdropper.

1) New Statistics: We derive the cumulative distribution functions (CDFs) of SINRs at the typical access point and the most detrimental eavesdropper that intercepts the transmission between the typical sensor and the access point in **Lemma 1** and **Lemma 2**, respectively.

Lemma 1: The CDF of SINR at the typical access point is derived as (6) *shown at the bottom of this page.*

Proof: See Appendix A. □

Lemma 2: The CDF of SINR at the most detrimental eavesdropper which intercepts the transmission between the typical sensor and the access point is derived as

$$F_{\gamma_{s,e}}(\gamma_{th}) = \exp\left\{ -\pi \lambda_e^s \int_0^\infty \exp\left\{ -\left(\lambda_s \rho_s + \lambda_{ap} \rho_{ap} \mu^{2/\alpha}\right)\pi \Gamma(1+2/\alpha)\Gamma(1-2/\alpha)(\gamma_{th})^{\frac{2}{\alpha}} t - \delta^2 \gamma_{th} t^{\alpha/2}/P_s \right\} dt. \right. \quad (7)$$

Proof: See Appendix B. □

2) Average Secrecy Rate: Based on our fundamental work in [24], the average secrecy rate between the sensor and the access point is the average of secrecy rate C_s^{ap} over $\gamma_{s,e}$ and γ_{ap}, which can be written as

$$\bar{C}_s^{ap} = \frac{1}{\ln 2} \int_0^\infty \frac{F_{\gamma_{s,e}}(x)}{1+x} (1 - F_{\gamma_{ap}}(x)) dx. \quad (8)$$

By substituting the CDF of γ_{ap} in (6) and the CDF of $\gamma_{s,e}$ in (7) into (8), we can obtain the average secrecy rate between the sensor and the access point.

Note that the derived average secrecy rate between the sensor and the access point in (8) is not in a simple form. As such, in the following corollary, we present the interference-limited

$$\begin{aligned} F_{\gamma_{ap}}(\gamma_{th}) = 1 - 2\pi\lambda_{ap}(1-\rho_{ap}) \int_0^\infty r \exp\left\{ -\left(\lambda_s\rho_s + \lambda_{ap}\rho_{ap}\mu^{\frac{2}{\alpha}}\right)\pi\Gamma(1+2/\alpha)\Gamma(1-2/\alpha)(\gamma_{th})^{\frac{2}{\alpha}} r^2 - \gamma_{th} r^\alpha \delta^2/P_s \right. \\ \left. - \pi\lambda_{ap}(1-\rho_{ap}) r^2 \right\} dr - 2\pi\lambda_{ap}(1-\rho_{ap}) \sum_{m=1}^{M-1} \frac{(r^\alpha)^m}{(-1)^m} \sum \frac{1}{\prod_{l=1}^{m} m_l! l!^{m_l}} \\ \times \int_0^\infty r \exp\left\{ -\left(\lambda_s\rho_s + \lambda_{ap}\rho_{ap}\mu^{\frac{2}{\alpha}}\right)\pi\Gamma(1+2/\alpha)\Gamma(1-2/\alpha)(\gamma_{th})^{\frac{2}{\alpha}} r^2 - \gamma_{th} r^\alpha \delta^2/P_s - \pi\lambda_{ap}(1-\rho_{ap}) r^2 \right\} \\ \times \left[-2/\alpha \left(\lambda_s\rho_s + \lambda_{ap}\rho_{ap}\mu^{\frac{2}{\alpha}}\right)\pi\Gamma(1+2/\alpha)\Gamma(1-2/\alpha)(\gamma_{th})^{2/\alpha} r^{(2-\alpha)} - \gamma_{th}\delta^2/P_s \right]^{m_1} \prod_{l=2}^{m} \\ \times \left[-\left(\lambda_s\rho_s + \lambda_{ap}\rho_{ap}\mu^{\frac{2}{\alpha}}\right)\pi\Gamma(1+2/\alpha)\Gamma(1-2/\alpha)(\gamma_{th})^{2/\alpha} \prod_{j=0}^{l-1} (2/\alpha - j) r^{2-l\alpha} \right]^{m_l} dr, \end{aligned} \quad (6)$$

where $\sum_{l=1}^{m} l \cdot m_l = m$.

case for the average secrecy rate with a single antenna at the access point.

Corollary 1: When the access points are equipped with single antenna in the interference-limited scenario, the average secrecy rate between the sensor and the access point is given by

$$\bar{C}_s^{ap} = \frac{\pi \lambda_{ap} \left(1-\rho_{ap}\right)}{\ln 2} \int_0^\infty \times \frac{\exp\left\{-\pi \lambda_e^s / \left(\Lambda_1 x^{2/\alpha}\right)\right\}}{(1+x)\left(\Lambda_1 x^{2/\alpha} + \pi \lambda_{ap}\left(1-\rho_{ap}\right)\right)} dx, \quad (9)$$

where $\Lambda_1 = \left(\lambda_s \rho_s + \lambda_{ap}\rho_{ap}\mu^{\frac{2}{\alpha}}\right)\pi\,\Gamma\left(1+2/\alpha\right)\Gamma\left(1-2/\alpha\right)$.

B. Average Secrecy Rate Between Access Point and Sink

Similar to (5), for a typical access point and its associated sink, the instantaneous secrecy rate is defined as

$$C_s^{sk} = [C_{sk} - C_{ap,e}]^+, \quad (10)$$

where $C_{sk} = \log_2(1+\gamma_{sk})$ and $C_{ap,e} = \log_2\left(1+\gamma_{ap.e}\right)$.

1) New Statistics: We derive the CDFs of SINRs at the typical sink and the most detrimental eavesdropper that intercepts the transmission between the typical access point and the sink in **Lemma 3** and **Lemma 4**, respectively.

Lemma 3: The CDF of SINR at the typical sink is derived as

$$\begin{aligned} F_{\gamma_{sk}}(x) = 1 &- 2\pi\lambda_{sk}\int_0^\infty r \exp \\ &\times \left\{-\lambda_{ap}\rho_{ap}\pi\,\Gamma\left(1+2/\beta\right)\Gamma\left(1-2/\beta\right)(\gamma_{th})^{\frac{2}{\beta}} r^2 \right. \\ &\left. - \gamma_{th} r^\beta \delta^2 / P_{ap} - \pi\lambda_{sk} r^2\right\} dr \\ &- 2\pi\lambda_{sk} \sum_{m=1}^{M-1} \frac{1}{(-1)^m} \sum \frac{1}{\prod_{l=1}^{m} m_l! l!^{m_l}} \int_0^\infty r^{\beta m+1} \exp \\ &\times \left\{-\lambda_{ap}\rho_{ap}\pi\,\Gamma\left(1+2/\beta\right)\Gamma\left(1-2/\beta\right)(\gamma_{th})^{\frac{2}{\beta}} r^2 \right. \\ &\left. - \gamma_{th} r^\beta \delta^2 / P_{ap} - \pi\lambda_{sk} r^2\right\} \\ &\left[- \lambda_{ap}\rho_{ap}\pi \frac{2}{\beta}\Gamma\left(1+2/\beta\right)\Gamma\left(1-2/\beta\right) \right. \\ &\left. \times (\gamma_{th})^{\frac{2}{\beta}} r^{2-\beta} - \gamma_{th}\delta^2/P_{ap}\right]^{m_1} \prod_{l=2}^{m} \\ &\times \left[- \lambda_{ap}\rho_{ap}\pi\,\Gamma\left(1+2/\beta\right)\Gamma\left(1-2/\beta\right)(\gamma_{th})^{\frac{2}{\beta}} \right. \\ &\left. \times \prod_{j=0}^{l-1} (2/\beta - j)\, r^{2-l\beta}\right]^{m_l} dr. \end{aligned} \quad (11)$$

Proof: See Appendix C. □

Lemma 4: The CDF of SINR at the most detrimental eavesdropper which intercepts the transmission between the typical access point and the sensor is derived as

$$\begin{aligned} F_{\gamma_{ap,e}}(x) = \exp\left\{-\pi\lambda_e^{ap}\int_0^\infty \exp\left\{-\lambda_{ap}\rho_{ap}\pi\,\Gamma\left(1+2/\beta\right)\right.\right. \\ \left.\left.\Gamma\left(1-2/\beta\right)\gamma_{th}{}^{\frac{2}{\beta}} t - \sigma^2\gamma_{th}t^{\beta/2}/P_{ap}\right\} dt\right\}. \end{aligned} \quad (12)$$

Proof: See Appendix D. □

2) Average Secrecy Rate: The average secrecy rate between the access point and the sink is the average of the secrecy rate C_s^{sk} over γ_{sk} and $\gamma_{ap,e}$, which is given by

$$\bar{C}_s^{sk} = \frac{1}{\ln 2}\int_0^\infty \frac{F_{\gamma_{sk}}(x)}{1+x}\left(1 - F_{\gamma_{ap,e}}(x)\right) dx. \quad (13)$$

By substituting the CDF of γ_{sk} in (11) and the CDF of $\gamma_{ap,e}$ in (12) into (13), we can obtain the average secrecy rate between the access point and the sink.

Note that the derived average secrecy rate between the access point and the sink is also not in a simple form, we present the interference-limited case for the average secrecy rate with single antenna at the access point in the following corollary.

Corollary 2: When the access points are equipped with single antenna in the interference-limited scenario, the average secrecy rate between the access point and the sink is given by

$$\bar{C}_s^{sk} = \frac{\pi\lambda_{sk}}{\ln 2}\int_0^\infty \frac{\exp\left\{-\pi\lambda_e^{ap}/\Lambda_2 x^{2/\beta}\right\}}{(1+x)\left(\Lambda_2 x^{2/\beta} + \pi\lambda_{sk}\right)} dx, \quad (14)$$

where $\Lambda_2 = \lambda_{ap}\rho_{ap}\pi\,\Gamma\left(1+2/\beta\right)\Gamma\left(1-2/\beta\right)$. *Based on* (14)*, for a specific target average secrecy rate* $\bar{C}_0$ *between the access point and the sink, the number of sinks must satisfy*

$$\lambda_{sk} > \bar{C}_0 \Lambda_2 \frac{\ln 2}{\pi\,\varepsilon}, \quad (15)$$

where $\varepsilon = \int_0^\infty \frac{\exp\left\{-\pi\lambda_e^{ap}/\left(\Lambda_2 x^{2/\beta}\right)\right\}}{(1+x)x^{2/\beta}} dx$.

C. Overall Average Secrecy Rate

In this subsection, we derive the overall average secrecy rate in three-tier WSNs. The instantaneous secrecy rate is defined as $C_s = \min\left(C_s^{ap}, C_s^{sk}\right)$. As such, the overall average secrecy rate is calculated as

$$\bar{C}_s = \int_0^\infty x\, f_{C_s}(x)\, dx = \int_0^\infty \left(1 - F_{C_s}(x)\right) dx, \quad (16)$$

where $f_{C_s}(x)$ and $F_{C_s}(x)$ is the probability density function (PDF) and the CDF of C_s, respectively. The CDF of C_s is calculated as

$$\begin{aligned} F_{C_s}(x) &= \Pr\left(\min\left(C_s^{ap}, C_s^{sk}\right) < x\right) \\ &= 1 - \Pr\left(\min\left(C_s^{ap}, C_s^{sk}\right) > x\right) \\ &= 1 - \Pr\left(C_s^{ap} > x\right)\Pr\left(C_s^{sk} > x\right). \end{aligned} \quad (17)$$

Substituting (17) into (16), we have

$$\bar{C}_s = \int_0^\infty \Pr\left(C_s^{ap} > x\right)\Pr\left(C_s^{sk} > x\right) dx, \quad (18)$$

where

$$\Pr\left(C_s^{ap} > x\right) = 1 - \int_0^\infty f_{\gamma_{s,e}}(t)\, F_{\gamma_{ap}}\left(2^x(1+t) - 1\right) dt \quad (19)$$

and

$$\Pr\left(C_s^{sk} > x\right) = 1 - \int_0^\infty f_{\gamma_{ap,e}}(t)\, F_{\gamma_{sk}}\left(2^x(1+t) - 1\right) dt. \quad (20)$$

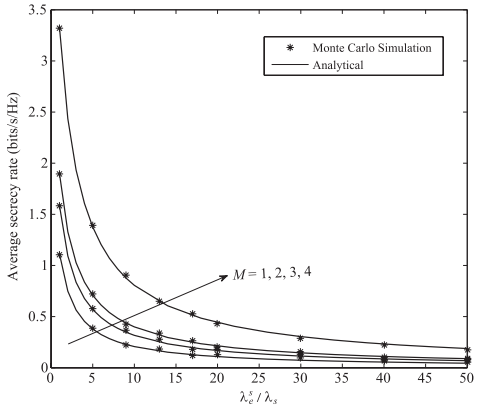

Fig. 2. The average secrecy rate versus $\frac{\lambda_e^s}{\lambda_s}$. $\lambda_s = 10^{-2}$, $\rho_s = 0.01$, $\lambda_{ap} = 10^{-2}$, $\rho_{ap} = 0.1$, $\alpha = 3.5$, $P_{ap} = 25$ dBm.

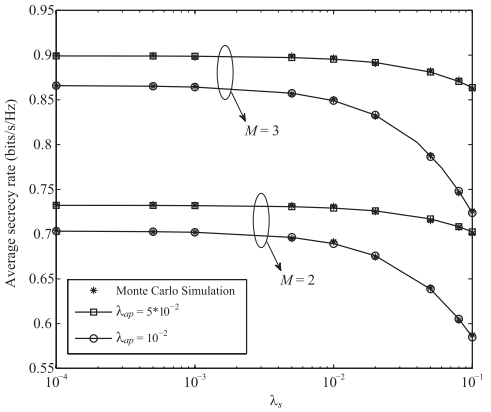

Fig. 3. The average secrecy rate versus λ_s. $\rho_s = 0.05$, $\rho_{ap} = 0.5$, $\lambda_e^s = 10^{-3}$, $\alpha = 3.5$, $P_{ap} = 25$ dBm.

Here, $f_{\gamma_{s,e}}$ is the derivative of $F_{\gamma_{s,e}}$ given in (7), and $f_{\gamma_{ap,e}}$ is the derivative of $F_{\gamma_{ap,e}}$ given in (12).

Unfortunately, the derived overall average secrecy rate between the sensor and the sink is not in a simple form, which motivates us to consider the interference-limited case with single antenna at the access point, as presented in the following corollary.

Corollary 3: When the access points are equipped with single antenna in the interference-limited scenario, the overall average secrecy rate between the sensor and the sink is given by

$$\bar{C}_s = \int_0^\infty \left[\int_0^\infty \frac{2\pi \lambda_e^s}{\alpha \Lambda_1 y^{2/\alpha+1}} \exp\left\{-\pi \lambda_e^s / \left(\Lambda_1 y^{2/\alpha}\right)\right\} \times \frac{\pi \lambda_{ap} \left(1-\rho_{ap}\right)}{\Lambda_1 (2^x (1+y)-1)^{2/\alpha} + \pi \lambda_{ap} \left(1-\rho_{ap}\right)} dy \right] \times \left[\int_0^\infty \frac{2\pi^2 \lambda_e^{ap} \lambda_{sk} \exp\left\{-\pi \lambda_e^{ap} / \Lambda_2 y^{2/\beta}\right\}}{\beta \Lambda_2 y^{2/\beta+1} \left(\Lambda_2 (2^x (1+y)-1)^{2/\beta} + \pi \lambda_{sk}\right)} dy \right] dx, \tag{21}$$

where $\Lambda_1 = \left(\lambda_s \rho_s + \lambda_{ap} \rho_{ap} \mu^{\frac{2}{\alpha}}\right) \pi \Gamma(1+2/\alpha) \Gamma(1-2/\alpha)$ *and* $\Lambda_2 = \lambda_{ap} \rho_{ap} \pi \Gamma(1+2/\beta) \Gamma(1-2/\beta)$.

IV. Numerical Examples

In this section, we present numerical examples to show the average secrecy rate of the three-tier WSN. We assume that the sensor's transmit power $P_s = 15$ dBm, the power spectral density of noise is -170 dBm/Hz, and the bandwidth is 1 MHz. We also assume that all the channel gains follow a complex Gaussian distribution with zero mean and unit variance. In all the figures, we see a precise match between the simulations and the exact analytical curves, which validate our analysis.

A. Average Secrecy Rate Between Sensor and Access Point

Fig. 2 plots the average secrecy rate between the sensor and the access point versus λ_e^s/λ_s. The analytical results are obtained from (8). We first see that the average secrey rate decreases with increasing the density of eavesdroppers that intercepts the transmission between sensor and access point, due to the detrimental effects of eavesdropping. We also see that the average secrecy rate increases with increasing the number of antennas at the access point, which results from the array again brought by using MRC at the access point.

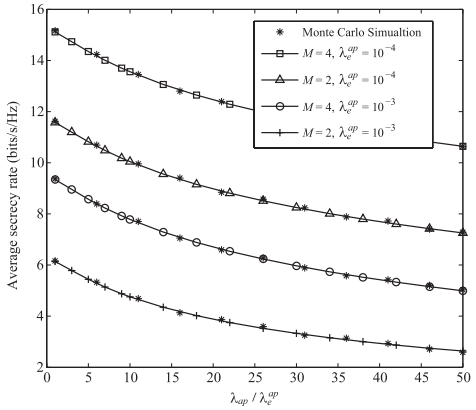

Fig. 4. The average secrecy rate versus $\frac{\lambda_{ap}}{\lambda_e^{ap}}$. $\rho_{ap} = 0.1$, $\lambda_{sk} = 10^{-2}$, $\beta = 3.5$, $P_{ap} = 15$ dBm.

Fig. 3 plots the average secrecy rate between the sensor and the access point versus λ_s for various λ_{ap} and M. The analytical results are obtained from (8). An interesting observation is that for the same number of antennas M, the average secrecy rate is nearly invariable for $\lambda_s < 2 \times 10^{-3}$, since the interference from other sensors is much smaller than the interference from the active access points, and slightly increasing the interference from the sensor imposes negligible effect on the performance. However, when $\lambda_s > 2 \times 10^{-3}$, the interference from other sensors is comparable with the interference from the active access points, and increasing the interference from the sensor degrades the secrecy performance. We also observe that increasing λ_{ap} increases the average secrecy rate. This is because with more access points, the distance between the typical sensor and the typical access point becomes shorter, which improves the average secrecy rate. In addition, we find that increasing λ_{ap} slows down the decreasing trend of average secrecy rate when λ_s increases.

B. Average Secrecy Rate Between Access Point and Sink

Fig. 4 plots the average secrecy rate between the access point and the sink versus $\lambda_e^{ap}/\lambda_{ap}$ for various λ_{ap} and M. The analytical results are obtained from (13). We first observe that the average secrecy rate decreases with increasing $\lambda_e^{ap}/\lambda_{ap}$, which indicates that more access points need to be

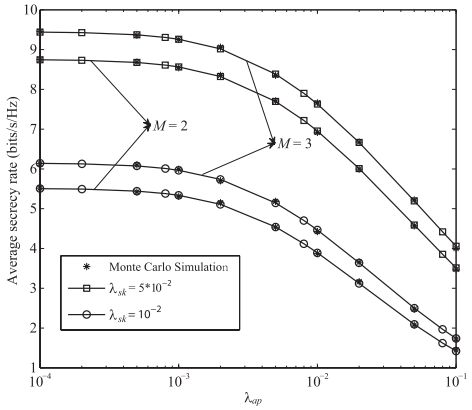

Fig. 5. The average secrecy rate versus λ_{ap}. $\rho_{ap}=0.1$, $\beta=3$, $\lambda_e^{ap}=10^{-3}$, $P_{ap}=25$ dBm.

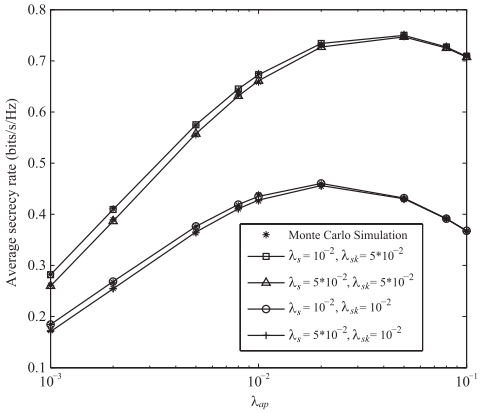

Fig. 6. The average secrecy rate versus λ_{ap}. $P_{ap}=30$ dBm, $M=2$, $\rho_s=0.01$, $\rho_{ap}=0.1$, $\alpha=2.8$, $\beta=3.2$, $\lambda_e^s=\lambda_e^{ap}=5*10^{-3}$.

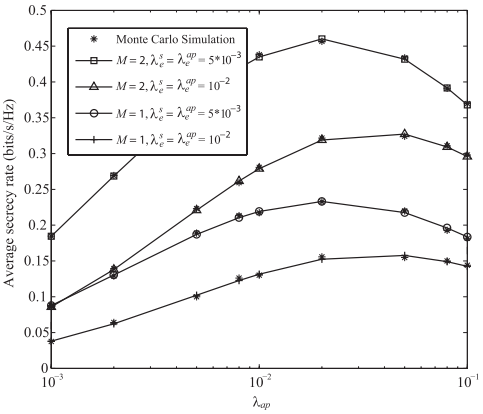

Fig. 7. The average secrecy rate versus λ_{ap}. $P_{ap}=30$ dBm, $\rho_s=0.01$, $\rho_{ap}=0.1$, $\alpha=2.8$, $\beta=3.2$, $\lambda_s=\lambda_{sk}=10^{-2}$.

deployed as the density of eavesdroppers increases, to combat eavesdropping. Second, with the same number of antennas at the access point, the average secrecy rate decreases with increasing λ_e^{ap}. The average secrecy rate between the access point and the sink improves with increasing the number of antennas at the access point M.

Fig. 5 plots the average secrecy rate between the access point and the sink versus λ_{ap} for various λ_{sk} and M. The analytical results are obtained from (13). We observe that the average secrecy rate alters slightly for $\lambda_{ap} < 2\times10^{-3}$, and decreases with increasing λ_{ap} for $\lambda_{ap} > 2\times10^{-3}$. This can be explained by the fact that for $\lambda_{ap} < 2\times10^{-3}$, the interference from the active access points is relatively small compared with the noise, and increasing the number of access points scarcely influence the performance. However, for $\lambda_{ap} > 2\times10^{-3}$, the interference from the access point imposes a dominant impact on the SINR between the access point and the sink, thus increasing the interference from the access points degrades the average secrecy rate. Another observation is that the average secrecy rate improves with increasing the density of sink, because the distance between the typical access point and the corresponding sink becomes shorter.

C. Overall Average Secrecy Rate

Fig. 6 plots the overall average secrecy rate versus λ_{ap} for various λ_s and λ_{sk}. The analytical results are obtained from (18). Interestingly, we find that the overall average secrecy rate first increases, and then decreases with increasing λ_{ap}, which implies that there exists an optimal λ_{ap} to achieve the maximum average secrecy rate. This phenomenon can be well explained by the tradeoff between the benefits brought by the shorter distance from the typical sensor to the typical access point and the detrimental effects caused by more interference from the active access points due to increasing λ_{ap}. It is also seen that the overall average secrecy rate can be improved by deploying more sinks, due to the shorter distance between the access point and the sink. It is further demonstrated that deploying more sensors in this network may not greatly degrade the average secrecy rate due to the low transmit power of sensors. More importantly, it is shown that the optimal λ_{ap} is more dependent on the λ_{sk}.

Fig. 7 plots the overall average secrecy rate versus λ_{ap} for various λ_e^s, λ_e^{ap} and M. The analytical results are obtained from (18). Similar as Fig. 6, we see that the overall average secrecy rate first increases, and then decreases with increasing λ_{ap}. As expected, the average secrecy rate decreases with increasing eavesdroppers. It is indicated that the optimal λ_{ap} for achieving the maximum average secrecy rate does not alter drastically with different λ_e^s and λ_e^{ap}.

V. Conclusion

We have analyzed the physical layer security of three-tier WSNs. We have examined the impact of random locations and spatial densities of sensors, access points, sinks, and external eavesdroppers on the secrecy performance. We have also obtained new expressions for the average secrecy rate. Based on our analysis, we have established the importance of physical layer security in three-tier WSNs, where our results support useful guidelines on secure transmission in practical WSNs. An important result is the minimum number of sinks required for a target average secrecy rate, which facilitates secure node deployment design in WSNs.

Appendix A
Proof of Lemma 1

From (1), the CDF of γ_{ap} is given by

$$F_{\gamma_{ap}}(\gamma_{th}) = \int_0^\infty \Pr\left[\frac{\left\|\mathbf{h}_{s_0,ap_0}\right\|^2 r^{-\alpha}}{In_{ap}+\delta^2/P_s} \le \gamma_{th}\right] f_{|X_{s_0,ap_0}|}(r)\,dr$$
$$= \int_0^\infty \Pr\left[\frac{\left\|\mathbf{h}_{s_0,ap_0}\right\|^2 \left|X_{s_0,ap_0}\right|^{-\alpha}}{In_{ap}+\delta^2/P_s} \le \gamma_{th}\right] 2\pi\lambda_{ap}$$

$$\times \left(1-\rho_{ap}\right) r \exp\left(-\pi \lambda_{ap}\left(1-\rho_{ap}\right) r^2\right) dr, \tag{A.1}$$

where $f_{|X_{s_0,ap_0}|}(r)$ is the PDF of the nearest distance between the access point and the typical sensor. The CDF of the access point SINR at distance r from its corresponding sensor is given as

$$\begin{aligned}
&\Pr\left[\frac{\left\|\mathbf{h}_{s_0,ap_0}\right\|^2 r^{-\alpha}}{In_{ap}+\delta^2/P_s} \le \gamma_{th}\right] \\
&= 1-\sum_{m=0}^{M-1}\frac{1}{m!}\mathbb{E}_{\Phi_{s,a}} \\
&\quad \times\left\{\mathbb{E}_{\Phi_{ap,a}}\left\{\int_0^{\infty}\left[\gamma_{th} r^{\alpha}\left(\tau+\delta^2/P_s\right)\right]^m \right.\right. \\
&\qquad \left.\left. \exp\left[-\gamma_{th} r^{\alpha}\left(\tau+\delta^2/P_s\right)\right] d\Pr\left(In_{ap}\le\tau\right)\right\}\right\}. \qquad \text{(A.2)}
\end{aligned}$$

We then substitute $\left(-\left(\tau+\delta^2/P_s\right)\gamma_{th}\right)^m e^{-\left(\tau+\delta^2/P_s\right)\gamma_{th}^{\{s\}} r^{\alpha}} = \left.\frac{d^m\left(e^{-\gamma_{th}x\left(\tau+\delta^2/P_s\right)}\right)}{dx^m}\right|_{x=r^{\alpha}}$ into (A.2), we rewrite the CDF of the access point SINR at distance r from its corresponding sensor as

$$\begin{aligned}
&\Pr\left[\frac{\left\|\mathbf{h}_{s_0,ap_0}\right\|^2 r^{-\alpha}}{In_{ap}+\delta^2/P_s} \le \gamma_{th}\right] \\
&= 1-\mathbb{E}_{\Phi_{s,a}}\left\{\mathbb{E}_{\Phi_{ap,a}}\left\{\int_0^{\infty}\exp\left[-\gamma_{th} r^{\alpha}\left(\tau+\delta^2/P_s\right)\right] d\Pr\right.\right. \\
&\qquad \left.\left.\times\left(In_{ap}\le\tau\right)\right\}\right\} - \sum_{m=1}^{M-1}\frac{(r^{\alpha})^m}{m!(-1)^m}\mathbb{E}_{\Phi_{s,a}} \\
&\quad \times\left\{\mathbb{E}_{\Phi_{ap,a}}\left\{\int_0^{\infty}\left.\frac{d^m\left(e^{-\gamma_{th}x\left(\tau+\delta^2/P_s\right)}\right)}{dx^m}\right|_{x=r^{\alpha}} d\Pr\right.\right. \\
&\qquad \left.\left.\times\left(In_{ap}\le\tau\right)\right\}\right\} \\
&= 1-\exp\left(-\gamma_{th} r^{\alpha}\delta^2/P_s\right)\mathcal{L}_{In_{ap}}\left(\gamma_{th} r^{\alpha}\right) \\
&\quad -\sum_{m=1}^{M-1}\frac{(r^{\alpha})^m}{m!(-1)^m}\left.\frac{d^m\left(\exp\left(-\gamma_{th}x\delta^2/P_s\right)\mathcal{L}_{In_{ap}}\left(\gamma_{th}x\right)\right)}{dx^m}\right|_{x=r^{\alpha}}. \qquad \text{(A.3)}
\end{aligned}$$

Remind that $I_{s,ap} = \sum_{i\in\Phi_{s,a}\setminus\{s_0\}}\left|\frac{\mathbf{h}_{s_0,ap_0}{}^{\dagger}}{\left\|\mathbf{h}_{s_0,ap_0}\right\|}\mathbf{h}_{i,ap_0}\right|^2\left|X_{i,ap_0}\right|^{-\alpha}$, using Slivnyak's theorem, the Laplace transform of $I_{s,ap}$ is

$$\begin{aligned}
&\mathcal{L}_{I_{s,ap}}(s) \\
&= \mathbb{E}_{\Phi_s}\left[\exp\left\{-s\sum_{i\in\Phi_{s,a}\setminus\{s_0\}}\left|\frac{\mathbf{h}_{s_0,ap_0}{}^{\dagger}}{\left\|\mathbf{h}_{s_0,ap_0}\right\|}\mathbf{h}_{i,ap_0}\right|^2\left|X_{i,ap_0}\right|^{-\alpha}\right\}\right] \\
&\overset{(a)}{=} \exp\left\{-2\pi\lambda_s\rho_s\int_0^{\infty}\left(1-\mathcal{L}_{\frac{\mathbf{h}_{s_0,ap_0}{}^{\dagger}}{\left\|\mathbf{h}_{s_0,ap_0}\right\|}\mathbf{h}_{i,ap_0}}\left(sy^{-\alpha}\right)\right)ydy\right\} \\
&\overset{(b)}{=} \exp\left\{-2\pi\lambda_s\rho_s\int_0^{\infty}\left(1-\frac{1}{1+sy^{-\alpha}}\right)ydy\right\} \\
&= \exp\left\{-\lambda_s\rho_s\pi\,\Gamma\left(1+2/\alpha\right)\Gamma\left(1-2/\alpha\right)s^{2/\alpha}\right\}, \qquad \text{(A.4)}
\end{aligned}$$

In (A.4), (a) follows from the generating functionnal of HPPP in [25], (b) follows from the fact that $\left|\frac{\mathbf{h}_{s_0,ap_0}{}^{\dagger}}{\left\|\mathbf{h}_{s_0,ap_0}\right\|}\mathbf{h}_{i,ap_0}\right|^2 \sim \exp(1)$.

Since $I_{ap,ap} = \mu\sum_{j\in\Phi_{ap,a}\setminus\{ap_0\}}\left|\frac{\mathbf{h}_{s_0,ap_0}{}^{\dagger}}{\left\|\mathbf{h}_{s_0,ap_0}\right\|}\mathbf{H}_{j,ap_0}\frac{\mathbf{h}_{j,sk_j}{}^{\dagger}}{\left\|\mathbf{h}_{j,sk_j}\right\|}\right|^2 |X_{j,ap_0}|^{-\alpha} = \mu\sum_{j\in\Phi_{ap}\setminus\{ap_0\}}H_j^{ap,ap}|X_{j,ap_0}|^{-\alpha}$, the Laplace transform of $I_{ap,ap}$ is

$$\begin{aligned}
&\mathcal{L}_{I_{ap,ap}}(s) \\
&= \exp\left(-\int\left[1-\mathbb{E}_h\left(\exp\left(-s\mu H_j^{ap,ap}y^{-\alpha}\right)\right)\right]\right. \\
&\qquad \left.\times\lambda_{ap}\rho_{ap}2\pi\,ydy\right) \\
&\overset{(c)}{=} \exp\left\{-\lambda_{ap}\rho_{ap}\pi\,\mu^{\frac{2}{\alpha}}\mathbb{E}_h\left\{\left(H_j^{ap,ap}\right)^{\frac{2}{\alpha}}\right\}\Gamma\left(1-\frac{2}{\alpha}\right)s^{\frac{2}{\alpha}}\right\} \\
&\overset{(d)}{=} \exp\left\{-\lambda_{ap}\rho_{ap}\pi\,\mu^{\frac{2}{\alpha}}\Gamma\left(1+2/\alpha\right)\Gamma\left(1-2/\alpha\right)s^{2/\alpha}\right\}, \qquad \text{(A.5)}
\end{aligned}$$

where (c) follows from the generating functionnal of HPPP in [25], (d) follows from $H_j \sim \exp(1)$.

With the Laplace transform of $I_{s,ap}$ and $I_{ap,ap}$, we derive the Laplace transform of In_{ap} as

$$\begin{aligned}
\mathcal{L}_{In_{ap}}(s) &= \mathcal{L}_{I_{s,ap}}(s)\,\mathcal{L}_{I_{ap,ap}}(s) \\
&= \exp\left\{-\left(\lambda_s\rho_s+\lambda_{ap}\rho_{ap}\mu^{\frac{2}{\alpha}}\right)\pi\,\Gamma\left(1+2/\alpha\right)\right. \\
&\qquad \left.\times\,\Gamma\left(1-2/\alpha\right)s^{2/\alpha}\right\}. \qquad \text{(A.6)}
\end{aligned}$$

Substituting (A.6) into (A.3), we obtain

$$\begin{aligned}
&\Pr\left[\frac{\left\|\mathbf{h}_{s_0,ap_0}\right\|^2 r^{-\alpha}}{In_{ap}+\delta^2/P_s} \le \gamma_{th}\right] \\
&= 1-\exp\left\{-\left(\lambda_s\rho_s+\lambda_{ap}\rho_{ap}\mu^{\frac{2}{\alpha}}\right)\pi\,\Gamma\left(1+2/\alpha\right)\right. \\
&\qquad \left.\times\,\Gamma\left(1-2/\alpha\right)\left(\gamma_{th}\right)^{2/\alpha}r^2-\gamma_{th}r^{\alpha}\delta^2/P_s\right\} \\
&\quad -\sum_{m=1}^{M-1}\frac{(r^{\alpha})^m}{m!(-1)^m}\left.\frac{d^m\left(V(x)\right)}{dx^m}\right|_{x=r^{\alpha}}, \qquad \text{(A.7)}
\end{aligned}$$

where $V(x) = \exp\left\{-\left(\lambda_s\rho_s+\lambda_{ap}\rho_{ap}\mu^{\frac{2}{\alpha}}\right)\pi\,\Gamma(1+2/\alpha)\,\Gamma(1-2/\alpha)(\gamma_{th}x)^{2/\alpha}-\gamma_{th}x\delta^2/P_s\right\}$.

We then apply the Faà di Bruno's formula to solve the derivative of mth order as follows:

$$\begin{aligned}
&\Pr\left[\frac{\left\|\mathbf{h}_{s_0,ap_0}\right\|^2 r^{-\alpha}}{In_{ap}+\delta^2/P_s} \le \gamma_{th}\right] \\
&= 1-\exp\left\{-\left(\lambda_s\rho_s+\lambda_{ap}\rho_{ap}\mu^{\frac{2}{\alpha}}\right)\pi\,\Gamma\left(1+2/\alpha\right)\right. \\
&\qquad \left.\times\,\Gamma\left(1-2/\alpha\right)\left(\gamma_{th}\right)^{2/\alpha}r^2-\gamma_{th}r^{\alpha}\delta^2/P_s\right\} \\
&\quad -\sum_{m=1}^{M-1}\frac{(r^{\alpha})^m}{(-1)^m}\sum\frac{1}{\prod_{l=1}^{m}m_l!l!^{m_l}}\exp \\
&\quad \times\left\{-\left(\lambda_s\rho_s+\lambda_{ap}\rho_{ap}\mu^{2/\alpha}\right)\pi\,\Gamma\left(1+2/\alpha\right)\Gamma\left(1-2/\alpha\right)\right. \\
&\qquad \left.\times\,\left(\gamma_{th}\right)^{2/\alpha}r^2-\gamma_{th}r^{\alpha}\delta^2/P_s\right\} \\
&\quad \left[-2/\alpha\left(\lambda_s\rho_s+\lambda_{ap}\rho_{ap}\mu^{2/\alpha}\right)\pi\,\Gamma\left(1+2/\alpha\right)\Gamma\left(1-2/\alpha\right)\right.
\end{aligned}$$

$$(\gamma_{th})^{\frac{2}{\alpha}} r^{(2-\alpha)} - \gamma_{th}\delta^2/P_s\Big]^{m_1} \prod_{l=2}^{m} \times \Big[-\left(\lambda_s \rho_s + \lambda_{ap}\rho_{ap}\mu^{2/\alpha}\right) \pi\, \Gamma\left(1+2/\alpha\right)\Gamma\left(1-2/\alpha\right) \times (\gamma_{th})^{\frac{2}{\alpha}} \prod_{j=0}^{l-1} (2/\alpha - j)\, r^{2-l\alpha}\Big]^{m_l}. \quad \text{(A.8)}$$

Substituting (A.8) into (A.1), we derive the CDF of γ_{ap} in (6).

Appendix B
Proof of Lemma 2

From (2), the CDF of $\gamma_{s,e}$ is given by

$$\begin{aligned} F_{\gamma_{s,e}}(\gamma_{th}) &= \Pr\left\{ \max_{e_k \in \Phi_{s,e}} \left\{ \frac{\left|h_{s_0,e_k}\right|^2 \left|X_{s_0,e_k}\right|^{-\alpha}}{In_{s,e} + \delta^2/P_s} \right\} \le \gamma_{th} \right\} \\ &\overset{(a)}{=} \exp\left\{ -\lambda_e^s \int_{R^2} e^{-\delta^2 \gamma_{th} \left|X_{s_0,e_k}\right|^{\alpha}/P_s} \mathcal{L}_{In_{s,e}} \times \left(\gamma_{th}\left|X_{s_0,e_k}\right|^{\alpha}\right) d\left|X_{s_0,e_k}\right| \right\} \\ &\overset{(b)}{=} \exp\left\{ -2\pi\lambda_e^s \int_0^{\infty} e^{-\delta^2\gamma_{th} r^{\alpha}/P_s} \mathcal{L}_{In_{s,e}} \times \left(\gamma_{th} r^{\alpha}\right) r dr \right\}, \end{aligned} \quad \text{(B.1)}$$

where (a) follows from the generating functionnal of HPPP in [25], (b) is obtained by converting cartesian coordinates to polar coordinates.

Using the generating functionnal of HPPP in [25], $\left|h_{i,e_k}\right|^2 \sim \exp(1)$, and $H_j^{ap,e} = \left| \mathbf{h}_{j,e_k} \frac{\mathbf{h}_{j,sk_j}{}^{\dagger}}{\left\|\mathbf{h}_{j,sk_j}\right\|} \right|^2 \sim \exp(1)$, we derive the Laplace transform of $I_{s,e}$ and $I_{ap,e}$ as

$$\begin{aligned} &\mathcal{L}_{I_{s,e}}(s) \\ &= \exp\left(-\int \left[1 - \mathbb{E}_h\left(\exp\left(-s\left|h_{i,e_k}\right|^2 y^{-\alpha} \right) \right) \right] \lambda_s \rho_s 2\pi y dy \right) \\ &= \exp\left\{ -\lambda_s \rho_s \pi\, \Gamma\left(1+2/\alpha\right)\Gamma\left(1-2/\alpha\right) s^{2/\alpha} \right\}, \end{aligned} \quad \text{(B.2)}$$

and

$$\begin{aligned} &\mathcal{L}_{I_{ap,e}}(s) \\ &= \exp\left(-\int \left[1 - \mathbb{E}_h\left(\exp\left(-s\mu H_j^{ap,e} y^{-\alpha} \right) \right) \right] \lambda_{ap}\rho_{ap} 2\pi y dy \right) \\ &= \exp\left\{ -\lambda_{ap}\rho_{ap}\pi\, \mu^{\frac{2}{\alpha}} \Gamma\left(1+2/\alpha\right)\Gamma\left(1-2/\alpha\right) s^{2/\alpha} \right\}, \end{aligned} \quad \text{(B.3)}$$

respectively.

With the Laplace transform of $I_{s,e}$ and $I_{ap,e}$, we derive the Laplace transform of $In_{s,e}$ as

$$\mathcal{L}_{In_{s,e}}(s) = \exp\left\{ -\lambda_s\rho_s\pi\,\Gamma\left(1+2/\alpha\right)\Gamma\left(1-2/\alpha\right) s^{2/\alpha} - \lambda_{ap} \times \rho_{ap}\pi\,\mu^{2/\alpha}\Gamma\left(1+2/\alpha\right)\Gamma\left(1-2/\alpha\right) s^{2/\alpha} \right\}. \quad \text{(B.4)}$$

Substituting (B.4) into (D.1), we derive the CDF of $\gamma_{s,e}$ in (7).

Appendix C
Proof of Lemma 3

From (3), the CDF of γ_{sk} is given by

$$F_{\gamma_{sk}}(\gamma_{th}) = \int_0^{\infty} \Pr\left[\frac{\left\|\mathbf{g}_{ap_0,Sk_0}\right\|^2 r^{-\beta}}{In_{ap,sk} + \delta^2/P_{ap}} \le \gamma_{th} \right] 2\pi\lambda_{sk} r \times \exp\left(-\pi\lambda_{sk} r^2\right) dr. \quad \text{(C.1)}$$

The CDF of the sink SINR at distance r from its corresponding access point is derived as

$$\begin{aligned} &\Pr\left[\frac{\left\|\mathbf{g}_{ap_0,sk_0}\right\|^2 r^{-\beta}}{In_{ap,sk} + \delta^2/P_{ap}} \le \gamma_{th} \right] \\ &= 1 - \sum_{m=0}^{M-1} \frac{1}{m!} \mathbb{E}_{\Phi_{ap,a}} \times \left\{ \int_0^{\infty} \left[\gamma_{th} r^{\beta} \left(\tau + \delta^2/P_{ap} \right) \right]^m \exp\left[-\gamma_{th} r^{\beta} \times \left(\tau + \delta^2/P_{ap} \right) \right] d\Pr\left(In_{ap,sk} \le \tau \right) \right\}. \end{aligned} \quad \text{(C.2)}$$

Note that $(-(\tau+\delta^2/P_{ap})\gamma_{th})^m e^{-(\tau+\delta^2/P_{ap})\gamma_{th}^{\{s\}} r^{\beta}} = \frac{d^m\left(e^{-\gamma_{th}x(\tau+\delta^2/P_{ap})}\right)}{dx^m}\Big|_{x=r^{\beta}}$, we rewrite (C.2) as

$$\begin{aligned} &\Pr\left[\frac{\left\|\mathbf{g}_{ap_0,sk_0}\right\|^2 r^{-\beta}}{In_{ap,sk} + \delta^2/P_{ap}} \le \gamma_{th} \right] \\ &= 1 - \mathbb{E}_{\Phi_{ap,a}} \left\{ \int_0^{\infty} \exp\left[-\gamma_{th} r^{\beta} \left(\tau + \delta^2/P_{ap} \right) \right] d\Pr \times \left(In_{ap,sk} \le \tau \right) \right\} - \sum_{m=1}^{M-1} \frac{\left(r^{\beta}\right)^m}{m!(-1)^m} \mathbb{E}_{\Phi_{ap,a}} \times \left\{ \int_0^{\infty} \frac{d^m\left(e^{-\gamma_{th}x\left(\tau+\delta^2/P_{ap}\right)} \right)}{dx^m}\Big|_{x=r^{\beta}} d\Pr\left(In_{ap,sk} \le \tau \right) \right\} \\ &= 1 - \exp\left(-\gamma_{th} r^{\beta} \delta^2/P_{ap} \right) \mathcal{L}_{In_{ap,sk}}\left(\gamma_{th} r^{\beta}\right) - \sum_{m=1}^{M-1} \frac{\left(r^{\beta}\right)^m}{m!(-1)^m} \frac{d^m\left(\exp\left(-\gamma_{th}x\delta^2/P_{ap}\right) \mathcal{L}_{In_{ap,sk}}\left(\gamma_{th}x\right) \right)}{dx^m}\Big|_{x=r^{\beta}}. \end{aligned} \quad \text{(C.3)}$$

Since $In_{ap,sk} = \sum_{j \in \Phi_{ap,a} \setminus \{ap_0\}} \left| \mathbf{g}_{j,sk_0} \frac{\mathbf{h}_{j,sk_j}{}^{\dagger}}{\left\|\mathbf{h}_{j,sk_j}\right\|} \right|^2 \left|X_{j,sk_0}\right|^{-\beta}$, using the generating functionnal of HPPP and $\left| \mathbf{g}_{j,Sk_0} \frac{\mathbf{h}_{j,sk_j}{}^{\dagger}}{\left\|\mathbf{h}_{j,sk_j}\right\|} \right|^2 \sim \exp(1)$, we derive the Laplace transform of $In_{ap,sk}$ as

$$\mathcal{L}_{In_{ap,sk}}(s) = \exp\left\{ -\lambda_{ap}\rho_{ap}\pi\,\Gamma\left(1+2/\beta\right)\Gamma\left(1-2/\beta\right) s^{2/\beta} \right\}. \quad \text{(C.4)}$$

Substituting (C.4) into (C.3), we obtain

$$\begin{aligned} &\Pr\left[\frac{\left\|\mathbf{g}_{ap_0,sk_0}\right\|^2 r^{-\beta}}{In_{ap,sk} + \delta^2/P_{ap}} \le \gamma_{th} \right] \\ &= 1 - \exp\left\{ -\lambda_{ap}\rho_{ap}\pi\,\Gamma\left(1+2/\beta\right)\Gamma\left(1-2/\beta\right) \times (\gamma_{th})^{2/\beta} r^2 - \gamma_{th} r^{\beta} \delta^2/P_{ap} \right\} \end{aligned}$$

$$- \sum_{m=1}^{M-1} \frac{\left(r^{\beta}\right)^{m}}{m!(-1)^{m}} \frac{d^{m}\left(U\left(x\right)\right)}{dx^{m}}\bigg|_{x=r^{\beta}} \tag{C.5}$$

with $U(x) = \exp\Big\{ - \lambda_{ap}\rho_{ap}\pi\,\Gamma(1+2/\beta)\Gamma(1-2/\beta)(\gamma_{th}x)^{2/\beta} - \gamma_{th}x\delta^{2}/P_{ap}\Big\}$.

We then apply the Faà di Bruno's formula to solve the derivative of mth order as follows:

$$\begin{aligned}
&\frac{d^{m}\left[\exp\left(U\left(x\right)\right)\right]}{dx^{m}}\bigg|_{x=r^{\beta}} \\
&= \sum \frac{1}{\prod_{l=1}^{m} m_{l}!l!^{m_{l}}} \exp\Big\{-\lambda_{ap}\rho_{ap}\pi\,\Gamma\left(1+2/\beta\right)\Gamma\left(1-2/\beta\right) \\
&\qquad\qquad \times \left(\gamma_{th}\right)^{2/\beta} r^{2} - \gamma_{th}r^{\beta}\delta^{2}/P_{ap}\Big\} \\
&\quad \times \Big[- \lambda_{ap}\rho_{ap}\pi\frac{2}{\beta}\Gamma\left(1+2/\beta\right)\Gamma\left(1-2/\beta\right) \\
&\qquad \times \left(\gamma_{th}\right)^{2/\beta} x^{2/\beta-1} - \gamma_{th}\delta^{2}/P_{ap}\Big]^{m_{1}} \\
&\quad \times \prod_{l=2}^{m}\Big[- \lambda_{ap}\rho_{ap}\pi\,\Gamma\left(1+2/\beta\right)\Gamma\left(1-2/\beta\right) \\
&\qquad\qquad \times \left(\gamma_{th}\right)^{2/\beta} \prod_{j=0}^{l-1}\left(2/\beta - j\right) x^{2/\beta-l}\Big]^{m_{l}}.
\end{aligned} \tag{C.6}$$

Based on (C.6), (C.5), and (C.1), we derive the CDF of γ_{sk} in (11).

APPENDIX D
PROOF OF LEMMA 4

From (4), the CDF of $\gamma_{ap,e}$ is given by

$$\begin{aligned}
F_{\gamma_{s,e}}\left(\gamma_{th}\right) &= \mathbb{E}_{\Phi_{ap,a}}\Bigg\{\mathbb{E}_{\Phi_{ap,e}}\Bigg\{\prod_{e\Phi_{ap,e}} \Pr\Bigg\{\frac{\left|g_{ap_0,e_k}\right|^{2}}{In_{ap,e}+\sigma^{2}/P_{ap}} \\
&\qquad \times \left|X_{ap_0,e_k}\right|^{-\beta} \le \gamma_{th}\Bigg|\Phi_{ap,a},\Phi_{ap,e}\Bigg\}\Bigg\} \\
&\overset{(a)}{=} \exp\Big\{-\lambda_{e}^{ap}\int_{R^{2}} e^{-\sigma^{2}\gamma_{th}\left|X_{ap_0,e_k}\right|^{\beta}/P_{ap}} \\
&\qquad \times \mathcal{L}_{In_{ap,e}}\Big(\gamma_{th}\left|X_{ap_0,e_k}\right|^{\beta}\Big)de\Big\} \\
&\overset{(b)}{=} \exp\Big\{ - 2\pi\,\lambda_{e}^{ap}\int_{0}^{\infty} e^{-\sigma^{2}\gamma_{th}r^{\beta}/P_{ap}} \\
&\qquad \times \mathcal{L}_{In_{ap,e}}\left(\gamma_{th}r^{\beta}\right) r\,dr\Big\},
\end{aligned} \tag{D.1}$$

where (a) follows from the generating functionnal of HPPP in [25], (b) is obtained by converting cartesian coordinates to polar coordinates.

Using the generating functionnal of HPPP in [25], we derive the Laplace transform of $I_{ap,e}$ as

$$\mathcal{L}_{I_{ap,e}}\left(s\right) = \exp\Big\{-\lambda_{ap}\rho_{ap}\pi\,\Gamma\left(1+2/\beta\right)\Gamma\left(1-2/\beta\right)s^{2/\beta}\Big\}. \tag{D.2}$$

Plugging (D.2) into (D.1), we derive the CDF of $\gamma_{s,e}$ in (12).

REFERENCES

[1] Y. Deng, L. Wang, M. Elkashlan, R. K. Mallik, and A. Nallanathan, "Secure multi-antenna transmission in three-tier wireless sensor networks," in *Proc. IEEE Global Telecommun. Conf. (GLOBECOM)*, Dec. 2015, pp. 1–5.

[2] I. F. Akyildiz, W. Su, Y. Sankarasubramaniam, and E. Cayirci, "A survey on sensor networks," *IEEE Commun. Mag.*, vol. 40, no. 8, pp. 102–114, Aug. 2002.

[3] A. D. Wyner, "The wire-tap channel," *Bell Syst. Tech. J.*, vol. 54, no. 8, pp. 1355–1387, 1975.

[4] H. V. Poor, "Information and inference in the wireless physical layer," *IEEE Wireless Commun.*, vol. 19, no. 1, pp. 40–47, Feb. 2012.

[5] G. Geraci, H. S. Dhillon, J. G. Andrews, J. Yuan, and I. B. Collings, "Physical layer security in downlink multi-antenna cellular networks," *IEEE Trans. Commun.*, vol. 62, no. 6, pp. 2006–2021, Jun. 2014.

[6] H. Wang, X. Zhou, and M. C. Reed, "Physical layer security in cellular networks: A stochastic geometry approach," *IEEE Trans. Wireless Commun.*, vol. 12, no. 6, pp. 2776–2787, Jun. 2013.

[7] Y. Pei, Y.-C. Liang, L. Zhang, K. C. Teh, and K. H. Li, "Secure communication over MISO cognitive radio channels," *IEEE Trans. Wireless Commun.*, vol. 9, no. 4, pp. 1494–1502, Apr. 2010.

[8] Y. Deng, L. Wang, S. A. R. Zaidi, J. Yuan, and M. Elkashlan, "On the security of large scale spectrum sharing networks," in *Proc. IEEE Int. Conf. Commun. (ICC)*, Jun. 2015, pp. 4877–4882.

[9] L. Dong, Z. Han, A. P. Petropulu, and H. V. Poor, "Improving wireless physical layer security via cooperating relays," *IEEE Trans. Signal Process.*, vol. 58, no. 3, pp. 1875–1888, Mar. 2010.

[10] Y. Zou, X. Wang, and W. Shen, "Optimal relay selection for physical-layer security in cooperative wireless networks," *IEEE J. Sel. Areas Commun.*, vol. 31, no. 10, pp. 2099–2111, Oct. 2013.

[11] X. He and A. Yener, "Two-hop secure communication using an untrusted relay: A case for cooperative jamming," in *Proc. IEEE Global Telecommun. Conf. (GLOBECOM)*, Dec. 2008, pp. 1–5.

[12] X. Zhou, R. K. Ganti, and J. G. Andrews, "Secure wireless network connectivity with multi-antenna transmission," *IEEE Trans. Wireless Commun.*, vol. 10, no. 2, pp. 425–430, Feb. 2011.

[13] X. Zhou, R. K. Ganti, J. G. Andrews, and A. Hjørungnes, "On the throughput cost of physical layer security in decentralized wireless networks," *IEEE Trans. Wireless Commun.*, vol. 10, no. 8, pp. 2764–2775, Aug. 2011.

[14] X. Zhang, X. Zhou, and M. R. McKay, "Enhancing secrecy with multi-antenna transmission in wireless ad hoc networks," *IEEE Trans. Inf. Forensics Security*, vol. 8, no. 11, pp. 1802–1814, Nov. 2013.

[15] Y. Deng, L. Wang, K.-K. Wong, A. Nallanathan, M. Elkashlan, and S. Lambotharan, "Safeguarding massive MIMO aided hetnets using physical layer security," in *Proc. Int. Wireless Commun. Signal Process. (WCSP)*, Oct. 2015, pp. 1–5.

[16] X. Li, M. Chen, and E. P. Ratazzi, "Array-transmission based physical-layer security techniques for wireless sensor networks," in *Proc. IEEE Int. Conf. Mechatron. Autom. (ICMA)*, Jul. 2005, pp. 1618–1623.

[17] S. Marano, V. Matta, and P. K. Willett, "Distributed detection with censoring sensors under physical layer secrecy," *IEEE Trans. Signal Process.*, vol. 57, no. 5, pp. 1976–1986, May 2009.

[18] R. Soosahabi and M. Naraghi-Pour, "Scalable PHY-layer security for distributed detection in wireless sensor networks," *IEEE Trans. Inf. Forensics Security*, vol. 7, no. 4, pp. 1118–1126, Aug. 2012.

[19] J. E. Barcelo-Llado, A. Morell, and G. Seco-Granados, "Amplify-and-forward compressed sensing as a physical-layer secrecy solution in wireless sensor networks," *IEEE Trans. Inf. Forensics Security*, vol. 9, no. 5, pp. 839–850, May 2014.

[20] H. S. Dhillon, R. K. Ganti, F. Baccelli, and J. G. Andrews, "Modeling and analysis of K-tier downlink heterogeneous cellular networks," *IEEE J. Sel. Areas Commun.*, vol. 30, no. 3, pp. 550–560, Apr. 2012.

[21] C.-H. Lee and M. Haenggi, "Interference and outage in Poisson cognitive networks," *IEEE Trans. Wireless Commun.*, vol. 11, no. 4, pp. 1392–1401, Apr. 2012.

[22] T. Kwon and J. M. Cioffi, "Random deployment of data collectors for serving randomly-located sensors," *IEEE Trans. Wireless Commun.*, vol. 12, no. 6, pp. 2556–2565, Jun. 2013.

[23] M. Yuksel and E. Erkip, "Diversity-multiplexing tradeoff for the multiple-antenna wire-tap channel," *IEEE Trans. Wireless Commun.*, vol. 10, no. 3, pp. 762–771, Mar. 2011.

[24] L. Wang, N. Yang, M. Elkashlan, P. L. Yeoh, and J. Yuan, "Physical layer security of maximal ratio combining in two-wave with diffuse power fading channels," *IEEE Trans. Inf. Forensics Security*, vol. 9, no. 2, pp. 247–258, Feb. 2014.

[25] D. Stoyan, W. S. Kendall, and J. Mecke, *Stochastic Geometry and Its Applications*, vol. 2. Hoboken, NJ, USA: Wiley, 1987.

Yansha Deng (S'13) received the Ph.D. degree in electrical engineering from the Queen Mary University of London, U.K., in 2015. She is currently a Postdoctoral Research Fellow with the Department of Informatics, King's College London, U.K.

Her research interests include massive MIMO, HetNets, molecular communication, cognitive radio, cooperative networks, and physical layer security.

Lifeng Wang (M'16) received the M.S. degree in electronics engineering from the University of Electronic Science and Technology of China, in 2012, and the Ph.D. degree in electronics engineering from the Queen Mary University of London, in 2015. He is currently a Postdoctoral Research Fellow with the Department of Electronic and Electrical Engineering, University College London. His research interests include millimeter-wave communications, massive MIMO, HetNets, cloud-RAN, cognitive radio, physical layer security, and wireless energy harvesting. He received the Exemplary Reviewer Certificate of the IEEE COMMUNICATIONS LETTERS in 2013. He has served as a TPC Member for many IEEE conferences, such as the IEEE GLOBECOM and ICC.

Maged Elkashlan (M'06) received the Ph.D. degree in electrical engineering from the University of British Columbia, Canada, in 2006. From 2007 to 2011, he was with the Wireless and Networking Technologies Laboratory, Commonwealth Scientific and Industrial Research Organization, Australia. During this time, he held an adjunct appointment with the University of Technology Sydney, Australia. In 2011, he joined the School of Electronic Engineering and Computer Science, Queen Mary University of London, U.K. He currently holds visiting faculty appointments with the University of New South Wales, Australia, and the Beijing University of Posts and Telecommunications, China. His research interests fall into the broad areas of communication theory, wireless communications, and statistical signal processing for distributed data processing, heterogeneous networks, and massive MIMO.

Dr. Elkashlan received the best paper award at the IEEE International Conference on Communications in 2014, the International Conference on Communications and Networking in China in 2014, and the IEEE Vehicular Technology Conference in 2013. He also received the Exemplary Reviewer Certificate of the IEEE COMMUNICATIONS LETTERS in 2012. He serves as an Editor of the IEEE TRANSACTIONS ON WIRELESS COMMUNICATIONS, IEEE TRANSACTIONS ON VEHICULAR TECHNOLOGY, and the IEEE COMMUNICATIONS LETTERS. He also serves as a Lead Guest Editor of the Special Issue on Green Media: The Future of Wireless Multimedia Networks of the *IEEE Wireless Communications Magazine* and the Special Issue on Millimeter Wave Communications for 5G of the *IEEE Communications Magazine*, and a Guest Editor of the Special Issue on Energy Harvesting Communications of the *IEEE Communications Magazine* and the Special Issue on Location Awareness for Radios and Networks of the IEEE JOURNAL ON SELECTED AREAS IN COMMUNICATIONS.

Arumugam Nallanathan (S'97–M'00–SM'05) was an Assistant Professor with the Department of Electrical and Computer Engineering, National University of Singapore, from 2000 to 2007. He served as the Head of Graduate Studies with the Faculty of Natural and Mathematical Sciences, King's College London, in 2011/2012. He is currently a Professor of Wireless Communications with the Department of Informatics, King's College London. He has coauthored over 250 papers in his research areas. His research interests include 5G technologies, millimeter-wave communications, cognitive radio, and relay networks. He was a corecipient of the best paper award at the 2007 IEEE International Conference on Ultra-Wideband. He is an IEEE Distinguished Lecturer.

He received the IEEE Communications Society SPCE Outstanding Service Award 2012 and the IEEE Communications Society RCC Outstanding Service Award 2014. He is an Editor of the IEEE TRANSACTIONS ON COMMUNICATIONS and the IEEE TRANSACTIONS ON VEHICULAR TECHNOLOGY. He was an Editor of the IEEE TRANSACTIONS ON WIRELESS COMMUNICATIONS (2006–2011), the IEEE WIRELESS COMMUNICATIONS LETTERS, and the IEEE SIGNAL PROCESSING LETTERS. He served as the Chair of the Signal Processing and Communication Electronics Technical Committee of the IEEE Communications Society, the Technical Program Cochair (MAC track) of the IEEE WCNC 2014, the Cochair of the IEEE GLOBECOM 2013 (Communications Theory Symposium), the IEEE ICC 2012 (Signal Processing for Communications Symposium), the IEEE GLOBECOM 2011 (Signal Processing for Communications Symposium), the IEEE ICC 2009 (Wireless Communications Symposium), and the IEEE GLOBECOM 2008 (Signal Processing for Communications Symposium), the Technical Program Cochair of the IEEE International Conference on UWB 2011, and the General Track Chair of the IEEE VTC 2008.

Ranjan K. Mallik (S'88–M'93–SM'02–F'12) received the B.Tech. degree from IIT Kanpur, in 1987, and the M.S. and Ph.D. degrees from the University of Southern California, Los Angeles, in 1988 and 1992, respectively, all in electrical engineering. From 1992 to 1994, he was a Scientist with the Defence Electronics Research Laboratory, Hyderabad, India, working on missile and EW projects. From 1994 to 1996, he was a Faculty Member of the Department of Electronics and Electrical Communication Engineering with IIT Kharagpur. From 1996 to 1998, he was a Faculty Member with the Department of Electronics and Communication Engineering, IIT Guwahati. Since 1998, he has been a Faculty Member with the Department of Electrical Engineering, IIT Delhi, where he is currently a Professor. His research interests are in diversity combining and channel modeling for wireless communications, space-time systems, cooperative communications, multiple-access systems, power line communications, difference equations, and linear algebra.

Dr. Mallik is a member of Eta Kappa Nu, the IEEE Communications, Information Theory, and Vehicular Technology Societies, the American Mathematical Society, and the International Linear Algebra Society, a fellow of the Indian National Academy of Engineering, the Indian National Science Academy, The National Academy of Sciences, India, Allahabad, the Indian Academy of Sciences, Bangalore, The World Academy of Sciences–for the advancement of science in developing countries, The Institution of Engineering and Technology, U.K., The Institution of Electronics and Telecommunication Engineers, India, and The Institution of Engineers (India), and a Life Member of the Indian Society for Technical Education. He has served as an Area Editor and Editor of the IEEE TRANSACTIONS ON WIRELESS COMMUNICATIONS and an Editor of the IEEE TRANSACTIONS ON COMMUNICATIONS. He is a recipient of the Hari Om Ashram Prerit Dr. Vikram Sarabhai Research Award in the field of electronics, telematics, informatics, and automation, and the Shanti Swarup Bhatnagar Prize in engineering sciences.